Applied Thermal Engineering 279 (2025) 127947

Contents lists available at ScienceDirect

Applied Thermal Engineering

journal homepage: www.elsevier.com/locate/ate

Research Paper

Design, commissioning and closed-loop operation of a high-temperature Brayton heat pump — CoBra

Fatma Cansu Yücel [a,*], Johannes Oehler [a], Maximilian Kriese [b], Enrico Jende [a], Nico Setzepfand [a], Panagiotis Stathopoulos [a]

[a] German Aerospace Center,Institute of Low-Carbon Industrial Processes, Cottbus, Germany

[b] German Aerospace Center, Institute of Low-Carbon Industrial Processes, Zittau, Germany

ARTICLE INFO

Keywords:
Brayton high-temperature heat pump
Turbo-machine driven high-temperature heat pump
Air as working fluid

ABSTRACT

This work presents the design, commissioning, and closed-loop operation of the high-temperature heat pump (HTHP) "CoBra", developed by the Institute of Low-Carbon Industrial Processes at the German Aerospace Center (DLR). CoBra is the first HTHP of its kind to implement a closed-loop reverse Brayton cycle using dry air as the working fluid. The system consists of a two-stage centrifugal compression unit, an axial turbine, and three shell-and-tube heat exchangers, with recuperation enabled, via a switchable 3/2-way valve. The compression and turbine systems are mounted on separate shafts, allowing for independent speed control and modular component replacement. The demonstrator was successfully operated in a closed-loop configuration for the first time in May 2024 and is now fully operational. Compressor outlet temperatures of up to 230 °C were reached. On the heat source side, turbine outlet temperatures of roughly −30 °C were feasible. However, during the commissioning experiments, presented in this current work, the cooling cycle was operated mostly at temperatures above 0 °C, due to a lack of insulation, which has been subsequently added to the system. The data presented in this work serves as proof-of-concept and shows that a closed-loop Brayton HTHP can deliver process heat and process cooling at industry-relevant temperature levels.

1. Introduction

Global energy demand has continued to grow steadily over the past decades. Today's global energy need is covered mainly by fossil fuels. Nevertheless, renewable energy systems have made significant progress by covering electricity demands up to 33.5% globally [1]. At the same time, heating is still dominated by fossil fuels and remains a major contributor to CO_2 emissions, accounting for to 50% [2], of which 24% originate from the industrial sector [3]. To reach the climate targets in 2030 and 2050, a major priority for the industrial sector is to decarbonize process heat. High-temperature heat pumps (HTHPs) are a promising technology suitable for delivering process heat above 150 °C [4] while enabling decarbonization through the use of electricity from renewable energy resources.

Several studies have examined the potential of HTHPs to decarbonize industrial heat and improve energy efficiency, both for existing and emerging technologies. Oehler et al. [5] provide an overview of power-to-heat technologies for process heat demand. The conversion ratio from electrical power to process heat varies greatly between different technologies, emphasizing the favorable conversion ratios of heat pumps compared to hydrogen-based alternatives [6]. Arpagaus et al. [7] identify processes in different industrial sectors with regard to their typical temperature ranges. Processes such as drying and distillation require process heat at temperatures above 200 °C, which includes sectors such as paper, food, beverage and chemicals. Regarding decarbonization options for industry, Bataille et al. [8] review options for aligning energy-intensive industry with the Paris Agreement [9]. They identify HTHPs as a low-carbon option for the generation of process heat at temperatures up to 250 °C. Moreover, industrial processes in the sectors mentioned above often produce waste heat, which is released to the environment, causing significant energy losses and reducing overall process efficiency. HTHPs can be used to recover and upgrade waste heat increasing both the system efficiency and the efficiency of the HTHP [10].

The vast majority of these production sites are supplied with heat by fossil fuels from centralized plants. Heat is then distributed at the plant via a distribution system, which generally uses steam or thermal oil as the heat transfer medium. To cover heat losses occurring during the distribution process, process heat is generated at higher temperatures than the actually required process temperatures. For these

* Corresponding author.
E-mail address: fatma.yuecel@dlr.de (F.C. Yücel).

https://doi.org/10.1016/j.applthermaleng.2025.127947
Received 24 May 2025; Received in revised form 27 July 2025; Accepted 15 August 2025
Available online 23 August 2025
1359-4311/

scenarios, HTHPs can serve as a drop-in boiler replacement especially since this approach does not require any major changes to the existing infrastructure and the sites. Waste heat sources of each individual unit within the site can be recorded, merged and fed centrally to an HTHP with a dedicated heat collection system.

Among the thermodynamic cycles considered for HTHPs, the reverse Brayton cycle – a gas-phase cycle using compression, heat rejection, expansion, and heat absorption – is of growing interest. It offers advantages such as the absence of phase change, a wide temperature range, and the use of environmentally-friendly working fluids like air or CO_2. However, it also faces important development challenges. These include relatively low coefficients of performance (COP) under high temperature lifts, complex turbomachinery requirements (e.g., high-speed compressors and expanders), and the need for durable, high-performance heat exchangers operating at elevated temperatures and pressures. In addition, system integration into industrial environments is limited due to the early maturity of this technology. Recent research has addressed these limitations through regenerative cycle configurations, improved component designs, and integration strategies. Despite current challenges, the reverse Brayton cycle remains a promising pathway for HTHPs in applications with stringent temperature and fluid requirements.

A range of manufacturers, e.g. Enerin, Olvondo, and Ecop are actively developing HTHP applications in industry [11–13]. While Enerin and Olvondo use Stirling-based cycles with helium as working fluid and piston compressors to reach temperatures above 200 °C, ECOP employs a reverse Brayton cycle with air and a rotating compressor. Furthermore, heat pump manufacturers, industrial sites as well as research institutes collaborate within several EU projects on the development of new HTHPs and their integration into existing processes [14,15]. DLR is participating in multiple EU funded projects such as SPIRIT, SOLINDARITY, and EEETHOS. The SPIRIT project aims to demonstrate of three full-scale HTHP technologies in two industrial sectors (paper and food [16]). It also seeks to improve the technical and economic performance of HTHPs to support broader market uptake. The SOLINDARITY project focuses on the integration of a solar energy-based heat upgrade system, which combines solar energy, HTHPs, thermal energy storage, and waste heat recovery to significantly reduce carbon emissions in the industrial sector [17]. The HTHPs implemented in this project are Brayton-based systems using air as working fluid. These three systems are based on the experience of the DLR with the CoBra pilot plant, the commissioning of which is presented in the current work. The EEETHOS project aims to develop technologies for energy efficient, flexible and decarbonized process heating for the drying and heating of minerals, including a reverse Brayton heat pump with supply temperatures up to 300 °C [18]. Another EU funded project with similar goals is Push2Heat [15]. Here, two electrically-driven heat pumps using vapor as working fluid as well as two thermally-driven heat pumps will be integrated into different industrial processes such as paper production and chemical industry.

The CoBra HTHP is an experimental facility which serves as a proof-of-concept for the feasibility of a closed-loop Brayton HTHP. It is also a basis for scale-ups such as on site integration projects as demonstrated in the SOLINDARITY project. In the following sections, the basic design followed by the step-by-step commissioning of the HTHP will be introduced. Finally, the first experimental data of the closed-loop operation of the CoBra will be presented.

2. The CoBra high temperature heat pump

The German Aerospace Center's (DLR) Institute for Low-Carbon Industrial Processes is (among other things) designing, developing and experimentally demonstrating HTHP systems providing heat sink temperatures up to 300 °C for industrial processes. One of these HTHPs is the **CoBra** heat pump, which is based on the **Bra**yton cycle utilizing air as working fluid and is located in **Co**ttbus (see Fig. 1).

Table 1
Key parameters of the CoBra heat pump demonstrator and the current setup.

Parameter	Design value	Current setup
pressure ratio (–)	6 to 7	2.5 to 3.5
mass flow rate (kg/s)	0.6 to 0.7	0.2 to 0.45
thermal power (kW): heat sink & heat source	100 to 200 & 25 to 55	20 to 60 & 5 to 20
max./min. temperature (°C): heat sink & heat source	350 &–40	260 &–30
COP (–)	1.25 to 1.35	1.3 to 1.4

The $T-s-$ diagram of the CoBra's ideal heat pump cycle is shown in Fig. 2. The process starts with an isentropic compression of the working fluid and the increase of temperature and pressure (1' → 2). Next, heat is rejected (isobarically) to the heat sink (2 → 3). The air (working fluid of the CoBra) is then guided through the recuperator for internal heat recovery to increase the compressor inlet temperature (1 → 1') and the coefficient of performance (COP). The pressurized, cooled air is then expanded through the turbine, which extracts work from the fluid (3' → 4) and cools it down further. Subsequently, the air absorbs heat q_{in} from the heat source before reentering the compression system (4 → 1).

The CoBra demonstrator has been designed to accommodate compressors and heat loads up to 200 kW of power and deliver process heat up to a temperature of 300 °C and process cooling down to temperatures of −60 °C. All design values were based on the compressor of a small turboshaft engine [19]. This compressor with a design pressure ratio of $\Pi = 6.3$ and a design power of $P = 200\,\text{kW}$ was intended to be the compressor for the CoBra but could not be successfully operated because of shaft dynamic problems and excitation of the compressor-drivetrain assembly. The current, alternative compression system has been chosen to match the turbine of the initial design. The CoBra in the scope of this work uses a two-stage centrifugal turbo-compressor system. A new compressor with a direct-drive will be implemented in 2025 to bring the CoBra to full capacity. Table 1 summarizes the specifications of the CoBra demonstrator for its original and its the design presented in the current work.

The CoBra demonstrator consists of a primary cycle, and two secondary cycles that simulate the industrial heat sink and source. Fig. 3 shows the piping and instrumentation diagram (P&ID) of the CoBra. The sections marked as ①, ② and ③ will be explained in Section 3.

The main components are the compression and turbine systems and the three shell-and-tube heat exchangers; the high-temperature heat exchanger (HTHX), the low-temperature heat exchanger (LTHX) and the recuperator. The setup was designed to allow for experimental freedom and modularity such that components can be easily replaced and tested individually. Therefore, the turbine and compression system are mounted on two separate shafts. The primary cycle is fed with dry air through the valve QMB15 using an external air drying system. A heater is mounted upstream of the compression system to allow for controlling the compressor inlet temperature and simulate an additional heat sink in future experiments. Downstream of the compression system a safety valve (FLB01) is installed, which is activated in case the system pressure increases above 7 bar. By switching the 2/3-way valve (RNB01) the CoBra can be operated with or without the recuperator. A bypass is mounted to enable a safe start-up of the CoBra and avoid compressor instabilities.

In the following sections the design process followed by the step-by-step commissioning of each component including the secondary cycles and additional infrastructure will be described in detail.

2.1. Compression system

The installed compression system was chosen according to the following three criteria:

Fig. 1. The CoBra demonstrator.

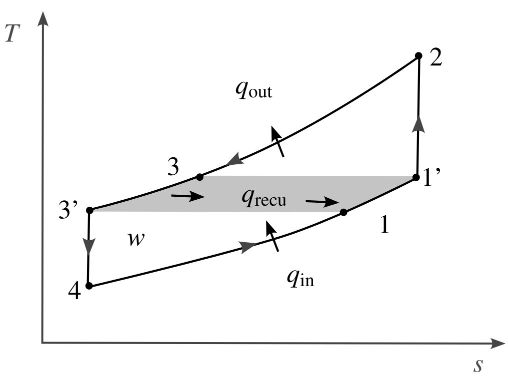

Fig. 2. $T-s$ Diagram of the ideal reverse Brayton cycle with recuperation.

- Minimum pressure ratio of 3 to realize output temperatures above 200 ° C at the heat sink and ensure turbine operation at choked conditions
- Off-the-shelve components to minimize operational risks and enable fast realization
- Compatibility to the existing infrastructure, most importantly aero-thermodynamically match the turbine

Following an evaluation of commercially available systems, a two-stage centrifugal compressor system from ASA Kompressor GmbH (hereinafter referred to as ASA) was selected, which are usually applied as superchargers for internal combustion engines. Fig. 4 shows a picture of the compression system. Air is sucked into the first stage compressor ① (ASA T1-520) [20] which has an aluminum impeller and housing. The housing is slightly modified to match the piping in the lab environment. The first stage is connected to the second ② (ASA T1-316) [21] via a compensator ③. The compensator is necessary to accommodate thermal expansion during operation and minimize the forces exerted on the compressors. Since a coupling of the motor and the, initially planned, high speed compressor has turned out to be the crux in the initial realization of the project, a belt-driven system ⑥ has been chosen as a temporary alternative for power transmission, while a detailed analysis of shaft dynamics of the original system has been carried out. This transmission system decouples vibration modes of the electric motor and the compression system allowing for more stability during operation. An intermediate shaft is used to connect the belt system with each compressor with two couplings. The entire system is mounted on a base plate ⑦, which sits on vibration dampers⑧.

The operation of the compression system is limited by the maximum allowable loading of the gearbox, which corresponds to a continuous output of 50 kW. For this reason, the pressure ratios of both stages were limited to remain within this loading limit. In addition, the transmission ratio for the belt drive of the second stage was adjusted. Transmission ratios of 2.55 for the first compressor stage and 2.68 for the second stage have been chosen, leading to an approx. 5% higher impeller speeds in the second stage. As a result, an equal distribution of power across both stages has been achieved for most of the operating range.

As originally intended for the application in supercharger systems, both compressors are manufactured using aluminum. However, steady-state simulations have shown that the resulting pressure ratio in conjunction with an increased inlet temperature for the second stage, outlet temperatures of up to 270 °C can be expected. According to the literature [22], the strength of aluminum decreases significantly at temperatures exceeding 100 °C. For this reason, the second stage has been modified by using a titanium alloy (Ti-6Al-4V) for the impeller. Moreover, the remaining components such as the vaned diffusor, the volute and the inlet housing are manufactured using stainless-steel (1.4305).

2.2. Heat exchangers

The heat exchangers were selected based on the specifications and design parameters of the initial design shown in Table 1. One key design objective was to minimize the pressure drop in the primary circuit of the heat pump, and keep a large surge margin for the compressors. To achieve this, three shell-and-tube heat exchangers were chosen, which are characterized by a very low pressure drop and very reliable tightness. However, downsides are a large design and hence, the increased amount of material, which needs to be heated up increasing the time until steady-state conditions are reached. Moreover, all heat exchangers introduce a large volume of air between the rotating turbo-machines, which could lead to compressor instabilities during transients. An inlet temperature of 15 °C was assumed at the heat sink secondary inlet, which resulted in an outlet temperatures of 100 °C of the HTHX. This value was used in the basic design of the turbine and other components. Once the design process was finalized, all three shell-and-tube heat exchangers were manufactured by an external company. Table 2 summarizes the main characteristics.

2.3. Turbine

The turbine was designed to fit the design parameters of the CoBra (see Table 1) at recuperated and unrecuperated conditions. Based on a

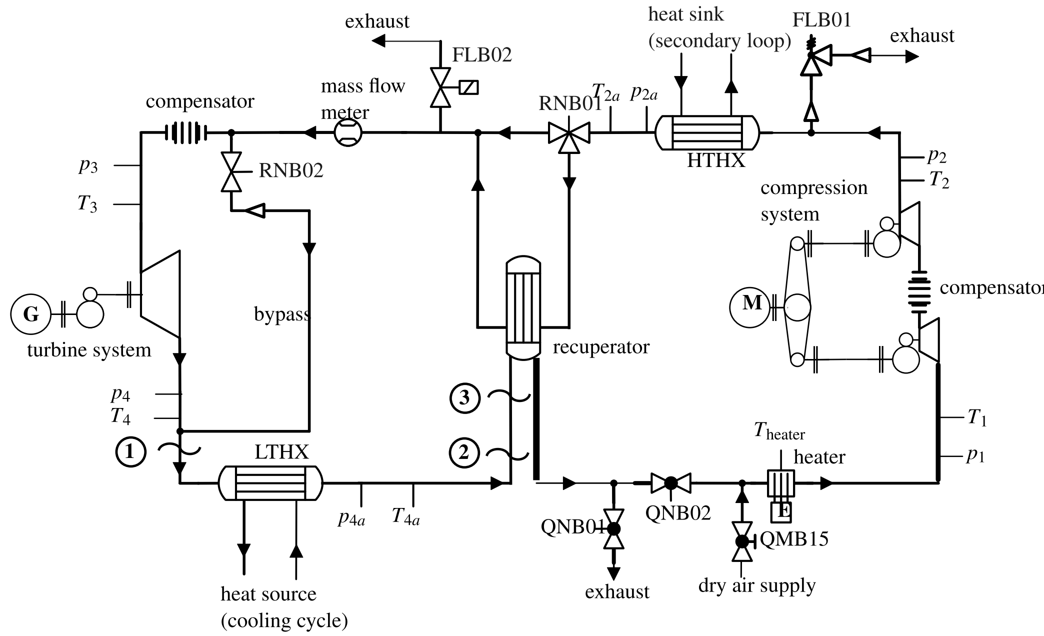

Fig. 3. P&ID of the CoBra heat pump demonstrator, the air is supplied via an air drying system connected to the valve QMB15.

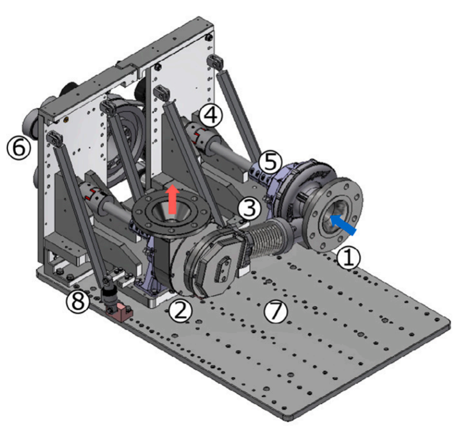

Fig. 4. The compression system.

Table 2
Specifications of the shell and tube heat exchangers.

	HTHX	LTHX	Recuperator
Type	Straight tube	Straight tube	U-tube
Working fluid	Air/ Air	Air/ Air	Air/ Air
Exchange surface (m^2)	100.4	100.4	71.8
Dimension (D × L, mm)	508 × 6882	508 × 6982	610 × 3766

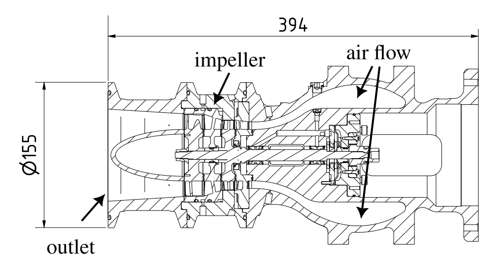

Fig. 5. Technical drawing of the two-stage axial turbine.

Table 3
Thermodynamic parameters of the turbine.

Parameter	Operation without recuperation	Recuperated operation
pressure ratio (–)	5.8	5.8
mass flow rate (kg/s)	0.665	0.665
inlet temperature T_3 (°C)	100	20
inlet pressure p_3 (bara)	6.1	6.1
power (kW)	93	71
isentropic efficiency (–)	91%	91%

series of thermodynamic simulations of the entire system, the required mass flow rate at chocking conditions, the nominal inlet temperature and pressure ratios have been determined at both, the recuperated and unrecuperated condition. The detailed aerodynamic design has been carried out by an external company specialized in detailed CFD simulation of turbo-machine systems (CFturbo GmbH). An isentropic efficiency of at least 85% has been demanded by the DLR for at the design operation condition. Once the first version of the aerodynamic design has been finalized a detailed design of the machine has been carried out by another company (AVL SCHRICK GmbH), which subsequently manufactured the turbine. The final design and dimensions of the two stage axial turbine are shown in Fig. 5, while its final design parameters are presented in Table 3.

2.4. Control system and data acquisition

The control system is split into two main units: the user interface in the control room, which receives commands from the operator and the available data from the system and the programmable logic controller (PLC), which runs all safety routines and transmits commands from the operator to the actuators. In reverse, data and status information from actuators and safety relevant sensors is sent from the PLC to the

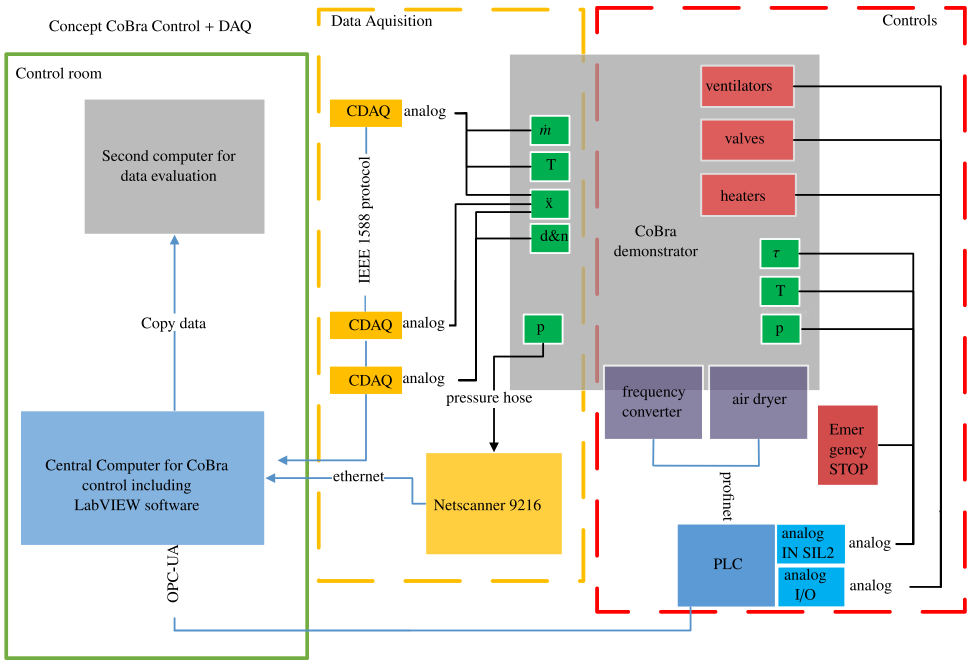

Fig. 6. Concept for control and data acquisition of the CoBra.

user interface. The communication between these units is established via an OPC-UA connection. This approach intents to combine a high level of safety by using a permanently active safety kernel and an easily exchangeable user interface to enable maximum adaptability of the system. Both systems need to work in order to operate the CoBra, while the PLC alone can bring the system to a safe standstill even if the computers in the control room do not work. The PLC runs with a cycle time below 50 ms, thus critical sensor readings and commands from the user interface are being updated at a rate of at least 20 Hz. The data acquisition system has over 100 channels. Some of them have high sampling rates of up to 500 kS/s depending on the sensor type and requirements. The operational tasks have been divided into:

- safety and controls: PLC
- precise and high-frequent data acquisition from sensors with high temporal resolution: Standard computer with National Instruments (NI) data acquisition hardware (3 CDAQs) and LabView software

The task distribution can be seen in Fig. 6. All actuators and sensors that are safety-relevant are connected to the PLC. High-frequency sensors, mostly for rotational speed and vibration measurements as well as the high precision thermodynamic sensors for pressure, mass flow and temperature are connected to the NI data acquisition system. All temperature measurements were conducted using type K thermocouples, while pressure data were acquired via a PSI NetScanner system. The mass flow in the Brayton cycle (primary circuit) was measured using a Coriolis flow meter (KROHNE OPTIMASS 6400C S100). The mass flow rate in the secondary cycles is measured by two flow meter sensors (SPINDLE). A detailed description of the sensors used and their accuracy can be found in **ASME-JO-2025 (accepted)**.

2.5. Additional infrastructure of demonstrator

The demonstrator is designed to deliver process heat an process cooling simultaneously. Therefore, it is designed to have two separate secondary cycles simulating a heat sink and a heat source. In addition an air drying system is necessary to provide dry air as working fluid under the required conditions.

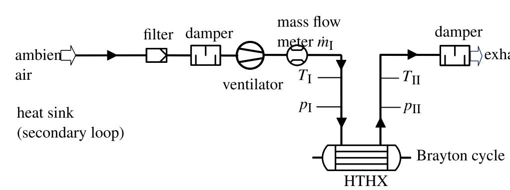

Fig. 7. Piping and instrumentation diagram of the heat sink secondary system.

2.5.1. Heat sink secondary system

Fig. 7 shows a simplified P&ID of the heat sink. The process parameters such as temperature, pressure and mass flow rate are designated in roman letters for the secondary systems. The heat sink simulates the cold stream of an industrial process that absorbs heat from the Brayton cycle. Air enters the secondary loop at ambient temperature and pressure and is released back to the environment at an elevated temperature after passing through the HTHX. The ventilator that circulates the air has a maximum capacity of 2000 m^3/h and can be operated at different frequencies allowing for varying the volumetric flow rate. A mass flow meter is mounted to measure the mass flow rate $\dot{m}_{\mathrm{I}}$ during operation. Two measurement flanges upstream (p_{I}, T_{I}) and downstream (p_{II}, T_{II}) the HTHX are installed, each equipped with a pressure and temperature sensor, respectively.

2.5.2. Heat source secondary system

Fig. 8 shows a simplified P&ID of the heat source secondary system. The air flow in the primary cycle has been expanded through the turbine and enters the LTHX through the diffusor at low temperature. The air in the secondary cycle is supplied by the air drying system to prevent ice formation due to very low temperatures. To feed the cooling cycle with dry air, the pipes are initially purged with a lobe pump with a volumetric flow rate of 5400 $m^{3/h}$. Temperature (T_{III}, T_{IV}) and pressure (p_{III}, p_{IV}) sensors are installed upstream and downstream the LTHX. Moreover, a mass flow meter is mounted to measure $\dot{m}_{\mathrm{II}}$ during operation. A heater equipped with an additional temperature sensor T_{heater} allows for controlling the temperature of the air flow before its entry into the LTHX.

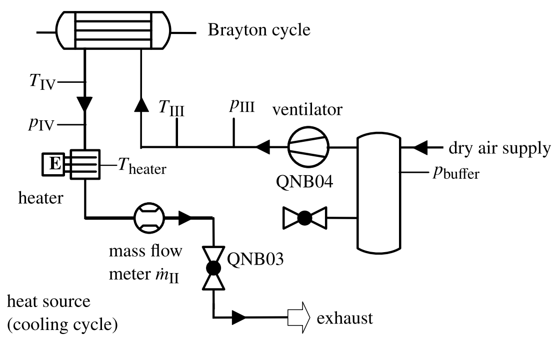

Fig. 8. Piping and instrumentation diagram of the heat source secondary system.

2.5.3. Air dryer

A system for air drying is used to continuously supply the heat pump system with dry air. This is necessary because none of the turbo-machines of the CoBra is hermetically sealed. At the same time, the turbine outlet temperatures are expected to be below the freezing point leading to water condensation and/or ice formation in the turbine and its diffusor. In the process-air drying system, ambient air is dried to a dew point below −50 °C and subsequently stored in a buffer tank at 8 bar. This buffer tank is connected to the Brayton cycle through the valve named "dry air supply" shown in Fig. 3. By closing valve QNB02 and opening the exhaust valve QNB01 the entire Brayton cycle can be purged with dry air. A similar system is in place for the heat source system, as mentioned earlier. During operation, the air from the buffer tank is used to maintain a constant pressure at the compressor inlet in the HTHP loop and compensate the small leakage in the turbo-machines.

3. Commissioning of the CoBra

In this section the step-by-step commissioning of the CoBra will be described. Turbo-machine components, both compressors and turbine, were first tested individually and subsequently connected within the Brayton cycle.

3.1. Compressor commissioning

As described in Section 2.1 two centrifugal compressors are operated in series to deliver the pressure and temperature levels required. Prior to the commissioning of the compression system, vibration tests are conducted. For this, multiple acceleration sensors are attached to the system including the bearings of the drive motor (eight sensors), the frame (14 sensors), the first stage compressor (four sensors), the second stage compressor (four sensors) as well as an additional eight sensors at the inlet casing of the second stage, respectively. These triaxial acceleration sensors measure the vibrations in all three spatial directions. In order to experimentally determine the resonance frequency at the respective positions an impact hammer equipped with an internal sensor to measure the applied force is used to stimulate the system. It is important to determine excitation areas at distinct positions, which are prone to vibration during operation.

The measured resonance frequencies are subsequently post-processed and visualized in a Campbell-diagram as a function of the motor speed. Fig. 10 shows an example Campbell-diagram of the coupling shaft, which was found to have the largest impact in terms of vibration excitation. The resonance frequencies of the compression system components can be seen on the left ordinate axis (black lines). For example, "stage 1" means that this natural mode of vibration is primarily characterized by a movement of the compressor stage 1. The linear graphs (red) marked as EO1 and EO2 (engine order 1 and 2) refer to the vibration excitation caused in particular by the intermediate shaft. The gray marked areas represent an accumulation of several resonance frequencies. It can be seen that there are various intersections of the natural frequencies with EO1 and EO2 when ramping up the motor speed. For example, at a speed of 5546 rpm, i.e. at the nominal operating point of the measurement shown below, an intersection between the second order and "stage 1" can be seen. Another example is the speed range from 4781 to 5100 rpm in which the first order has intersections with "stage 2" in the entire speed range. These intersection indicate so-called crossings, which can lead to an amplification of the resonances and hence, cause an elevated vibration damaging the respective component. Ideally these resonance frequencies should be avoided during operation as well as during the start-up and shut-down procedure. This method helps to predict these frequencies and enables a safe operation of the system. At the same time, the acceleration sensors are used to monitor the vibration of the system at high sample rates during operation. To prevent components from damage an emergency shut-down is initiated once the vibration value exceeds 15 mm/s.

Based on the results of the modal analysis the compression system was commissioned in two stages. At first, the second stage compressor was operated alone, followed by the operation of both compressors in series. The goal of these tests is to evaluate the compressors' performance in their current installation situation. The experimental setup is shown schematically in Fig. 9. For the test of the second stage compressor, the first stage (including its drive belt) and the compensator were dismounted. The compressor is driven by an electric motor with a drive power of up to 320 kW and a maximum speed of 3000 rpm. The motor's shaft is connected to the compressor via a belt system, an intermediate shaft and a gearbox with a transmission ratio of 1:15 (see Fig. 9 (left)). The compressor inlet is realized through the Coriolis mass flow meter and a flexible hose. Pressure transducers and thermocouples are mounted at the compressor inlet (T_1, p_1) and outlet (T_2, p_2). A control valve is installed downstream of the compressor to gradually increase the back pressure and test different operating points along the compressor's speed lines. Once the performance map measurement of the second stage has been successfully completed, the first stage has been installed, to operate both compressors in series, as shown in Fig. 9 (right). In addition to the pressure sensors mounted at the inlet and outlet of the compression system two pressure sensors p_{1a} and p_{1b} are mounted in the inlet casing of the second stage compressor to help determine the pressure ratios of the individual stages.

Fig. 11 and Fig. 12 show the compressor maps provided by the manufacturer for the first and second stage overlaid with the calculated and measured operation points. The calculations have been carried out based on the manufacturer's compressor map and the pressure and temperature measurements at the inlet of each compressor. The black lines indicate the speed lines measured by the manufacturer. The measurements in the lab environment are conducted for a constant motor speed of 2175 rpm which corresponds to a compressor speed of 80.000 rpm when considering slippage in the belt drive system and a varying choke opening. The slippage is around 1,4 to 1,6% at this operating point. The calculation has been conducted using the rotational speed of the intermediate shaft which means that the slip has been measured. Fig. 11 show the measurements values obtained when both compressors are mounted in series. Fig. 12 shows the values for the second stage when operated stand-alone. As mentioned, the operating point for the first compressor stage is calculated using $\dot{m}$, p_1, T_1, p_{1a} and p_{1b}. For the second stage T_{1a} is used instead of T_1 for the inlet conditions and p_2 is used for the outlet pressure. The pressure between both stages is assumed to be the mean value of both p_{1a} and p_{1b}. For the first stage compressor the measured and calculated values align well with the constant speed line provided by the manufacturer. For the second stage, however, it is notable that the calculated values are lower compared to the speed line in the compressor map. This is due to the fact that the air enters the second stage at higher temperature and pressure conditions.

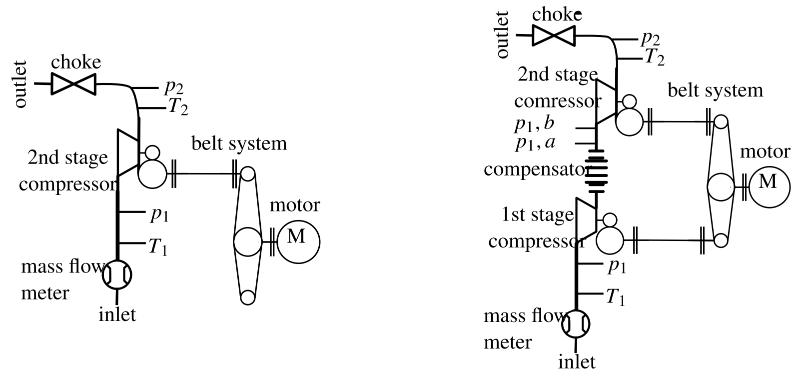

Fig. 9. Experimental setup for the commissioning of the second stage compressor (left) and both compressors in series (right).

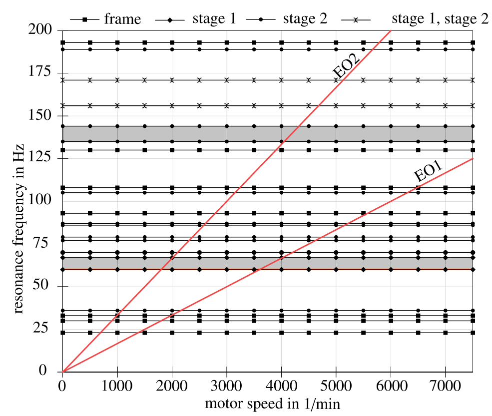

Fig. 10. Campbell diagram of the coupling shaft.

Moreover, there is a discrepancy visible between the calculated and measured values. The duct between the first compressor's outlet and the second compressor's inlet casing is the main differences from the usual compressor's operating conditions with free inflow and a choke at the outlet. Presumably, the geometry of the inlet casing and non-optimal inflow conditions of the second stage are responsible for the additional pressure loss. The live-tracking of the compressor operating points similar to Fig. 11 is visualized during operation to help prevent the compressors from surge and choke.

3.2. HTHX and heat sink

The setup for the commissioning of the HTHX including the heat sink is visualized in Fig. 13, while the system was operated in an open loop. The mass flow of the heat sink (secondary) was controlled using the ventilator. To simulate the turbine and gradually increase the compressor back pressure, a control valve was installed downstream of the HTHX. The mass flow meter in the Brayton cycle was installed upstream of the compressors like in the previous compressor tests, but has later been relocated to the high pressure leg before the choke valve. This helped to avoid noise emissions from the flow meter due to high volumetric flows in the low pressure air inlet. In addition, the design conditions of the flow meter are high densities of about $5\,\mathrm{kg/m^3}$ since it has been designed to operate upstream the turbine in the high pressure leg.

During the experiments the motor speed was increased gradually while avoiding sharp temperature gradients exceeding $\frac{\delta T_2}{\delta t}$ in the HTHX. This temperature gradient can also be seen in Fig. 14 (D) where the green line shows the compressor outlet temperature T_2. The sink mass flow can be set to values in the interval of 0.19..0.63 kg/s.

3.3. Turbine

Before operating the turbine within the CoBra an initial testing has been conducted by the manufacturer. In these tests, no power has been generated, but instead pressurized air was guided into the turbine inducing its rotation up to its design speed of $n_{\mathrm{turbine,design}} = 63\,000\,\mathrm{rpm}$ to ensure mechanical integrity and low vibrations. After the installation of the turbine within the CoBra's Brayton loop, an experimental modal analysis has been conducted to identify potentially harmful resonance frequencies. The outcome of this analysis confirmed the operational instructions of the manufacturer that the turbine should not be operated at rotational speeds 50–55 krpm for an elongated period of time. After evaluation of the modal analysis, the turbine was brought up to a speed of $n_{\mathrm{turbine}} = 59\,880\,\mathrm{rpm}$ by using the generator as a motor drive. These tests confirmed the mechanical integrity of the turbine and did not reveal any additional harmful resonance frequencies. The setup for the commissioning of the turbine is visualized in Fig. 3 (up to point ①).

Before testing the turbine in power generation mode, several simulations were performed with a calibrated transient thermodynamic model of the entire heat pump, using the simulation tool MODELICA [23]. These simulations provided all necessary information for the definition of a safe ramp-up and operation of the system in an open-loop, while at the same time avoiding the risk of turbine icing. A similar study has been performed in the past for the original design of the CoBra [24].

The CoBra turbine is designed for inlet temperatures between $T_3 =$ 15 °C up to 100 °C. Once the turbine is extracting work from the flow, its outlet temperature T_4 can drop well below freezing temperatures. In a closed-loop operation dry air is used to avoid condensation or icing. For the turbine commissioning experiments the heat pump has been operated in an open-loop (see Fig. 3 up to point ①) with ambient, humid air passing through the turbine. Several simulations were conducted with varying turbine input parameters. They aimed in identifying the turbine inlet conditions that resulted in turbine exit temperatures T_4 above 0 °C. The resulting operating conditions required a high pressure ratio and high work extraction in the turbine and potentially a large temperature drop. The beginning of each experiment, when components like the HTHX are at ambient temperature and thus $T_3 \approx T_0$, has been identified as most critical for turbine (outlet) icing. In order to avoid this, the optimal start-up commands have been chosen as visualized in Fig. 14 (A) and (B). For both, simulation and experiments, the boundary conditions are chosen to be as following:

- ambient temperature $T_0 = 15$ °C (this is also the initial temperature of HTHX and pipes)
- compressor inlet temperature $T_1 = 15$ °C (in the experiment 14.5–17.0 °C)
- secondary mass flow $\dot{m}_I = 0{,}2\,\mathrm{kg/s}$ which corresponds to the minimal possible mass flow at 15 Hz ventilator speed

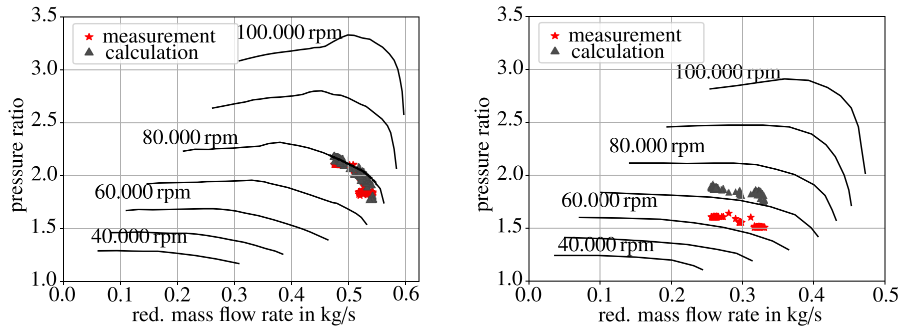

Fig. 11. Compressor map provided by the manufacturer for the first stage (left) and second stage compressor (right) overlaid with the calculated and measured operating point for a constant motor speed of 80.000 rpm.

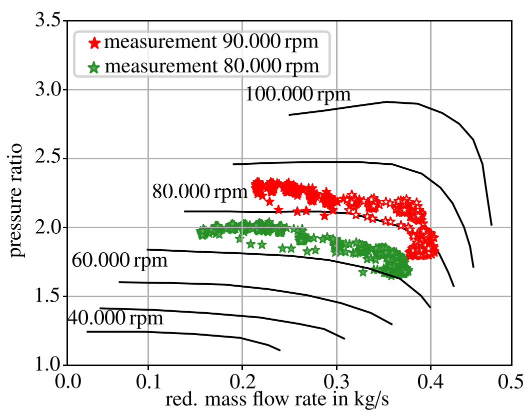

Fig. 12. Compressor map provided by the manufacturer for the second stage compressor overlaid with the measured operating point for a constant motor speed of 80.000 rpm and 90.000 rpm.

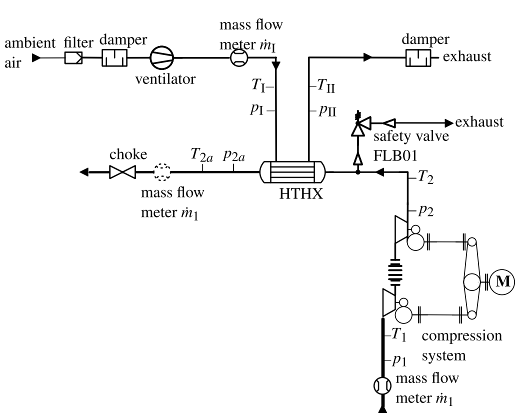

Fig. 13. Setup of the CoBra demonstrator for commissioning of the HTHX including the heat sink.

Fig. 14 (C) shows the results of the optimized simulation where turbine outlet temperatures below zero can be avoided during the start-up maneuver. The turbine-bypass is fully open initially to increase the overall mass flow rate and simultaneously reduce the pressure ratio of the compressors. The maximum mass flow rate is limited by the compressor's choke line. The most important measure to avoid low turbine outlet temperatures T_4 is the turbine speed. Hence, only after the turbine inlet temperature has surpassed a value of T_3 = 30 °C, the generator speed is increased to a value of 750 rpm which corresponds to a turbine speed of 15 krpm. This allows the turbine to extract more work from the fluid causing a greater temperature drop. The extracted turbine work can be estimated from the difference between T_3 and T_4 in Fig. 14 (D). At the end of the start-up simulation the generator speed is increased (black line in Fig. 14 (A)) to reach maximum efficiency values of the turbine, which results in turbine exit temperature T_4 below zero. As mentioned earlier, temperatures below the freezing point were avoided in the open-loop configuration and therefore, the generator speed was kept in the experiment at lower levels.

Fig. 14 (B) shows the actual commands during the experiment. The duration of the presented experiment of 3,5 h is longer compared to the simulation but the system generally shows the same pattern. The compressor speed is increased slowly over time, with small steps instead of the simulation's slope. The bypass opening has been reduced to 80% at a compressor speed of 1075 rpm instead of 1553 rpm in the simulation. This was necessary because compressor choking was detected in the compressor map (see Fig. 11). Moreover, the elevated sound emission from the compressors led to the decision of closing the bypass earlier. Both, simulation (Fig. 14 (C)) and experiment (Fig. 14 (D)) show the same trend for the compressor outlet temperature T_2 rising almost instantly with any increase in compressor speed. T_3 rises more gradually due to the large inertia of the HTHX. T_2 can be kept above zero during start-up and at the end of the experiment it was possible to increase turbine speed and extract a considerable amount of work from the fluid. The effect of a turbine speed increase on T_4 can be clearly seen e.g. in the simulation at a time stamp of 3900 s and 7100 s and in the experiment at 3700 s and 9800 s. An increase of the turbine speed results in a sudden drop in turbine outlet temperature T_4 and thus, more work extracted from the turbine.

3.4. LTHX and heat source

The experimental setup for the commissioning of the LTHX including the heat source is visualized in Fig. 8 up to point ②. For this last commissioning step the CoBra was operated in an open loop. Hence, the compressor inlet pressure p_1 and turbine outlet pressure p_4 correspond to ambient pressure. After exiting the turbine the air flow is guided through the LTHX where heat is absorbed from the heat source increasing the LTHX outlet temperature T_{4a}. The ventilator applied in the heat source cycle (see Fig. 8) can deliver a secondary mass flow rate in the range of m_{II} = 0.40 to 1.33 kg/s at temperatures of T_{III} =15 °C to 40 °C. Both values can be controlled individually using the heater and ventilator in the heat source cycle, respectively. After successfully commissioning the LTHX including the heat source, the CoBra was operated in a closed-loop cycle for the first time. The experimental results will be discussed in Section 4.

4. Closed-loop operation

4.1. Start-up and shut-down procedure

Once the commissioning of the individual components has been concluded in open loop, the heat pump loop has been closed. The

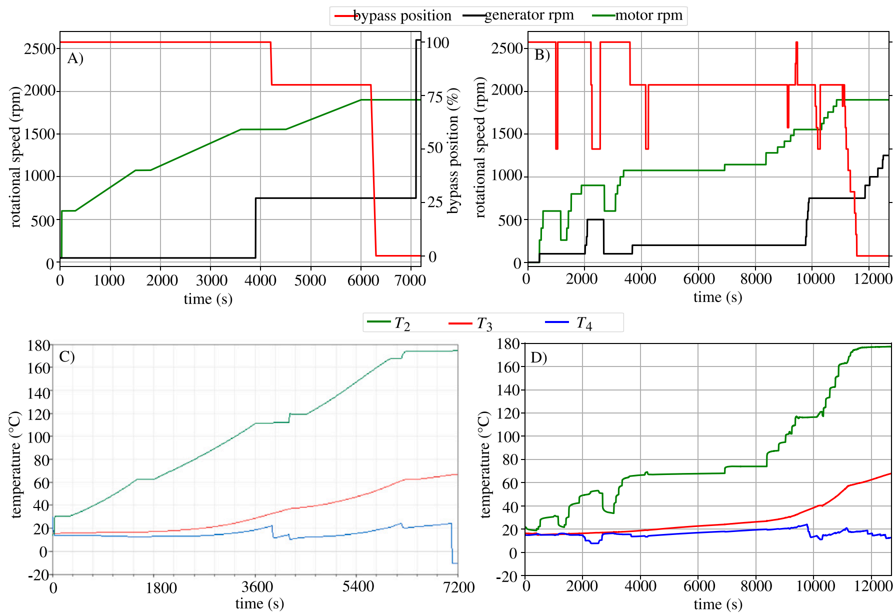

Fig. 14. Simulation and experimental data of the open-loop commissioning of the turbine using compressors and HTHX for inlet air conditioning.

Table 4
Motor and generator speed during the start-up procedure.

Motor speed (rpm)	260	400	600	800	950	1075
Generator speed (rpm)	200	500	800	1000	1200	1300

experiments in closed loop always started with a purge of the Brayton and the heat source cycles with dry air. Dew point sensors monitor the air humidity during purging and operation.

In a next step, the oil pumps for the turbo-machines are started and once a sufficient oil pressure as well as a low dew point is reached, the compression and turbine systems are started. The motor and the generator speeds are increased in a stepwise manner as shown in Table 4. These values have been carefully chosen to avoid any resonance frequencies as mentioned in Section 3.1, while maintaining a nearly constant speed-ratio between the two turbo-machines. The vibration values are monitored throughout the experiment.

The motor and generator speed is increased by an increment of 100 rpm while ensuring a hold time of several minutes at each new speed step to allow for temperature adjustment of the heat exchangers and avoid large temperature gradients. After reaching a motor speed of 600 rpm, the ventilators in the heat source and sink are activated. The motor speed of 1075 rpm corresponds to a compressor speed of 40.000 rpm for the first compressor stage.

The shut-down procedure is equivalent to the start-up. The motor and generator speeds are decreased incrementally according to Table 4.

4.2. First full closed-loop operation of the CoBra

Due to limitations in the maximum power consumption of the compression system, the CoBra can be operated up to a maximum compressor power of $P_C = 75\,\text{kW}$. Fig. 15 illustrates the heat transfer to the HTHX $\dot{Q}_{\text{HTHX,in}}$ (red) and LTHX (blue), as well as the heat flow delivered to the heat sink $\dot{Q}_{\text{HTHX,out}}$ (pink). Moreover, the fluid power of the compressor (green), the turbine (orange) and the COP (black) are shown over the entire duration of the experiment (≈7.5 h). As

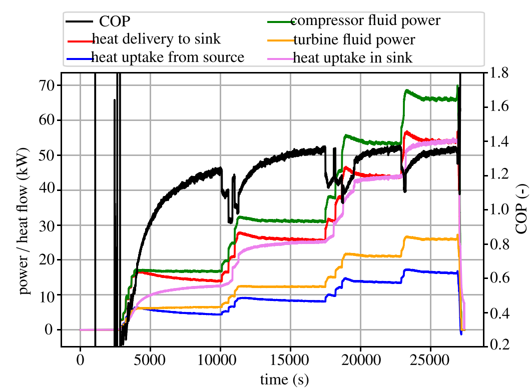

Fig. 15. Closed-loop operation of the CoBra. COP, fluid power and heat flux evolution over the entire operation duration.

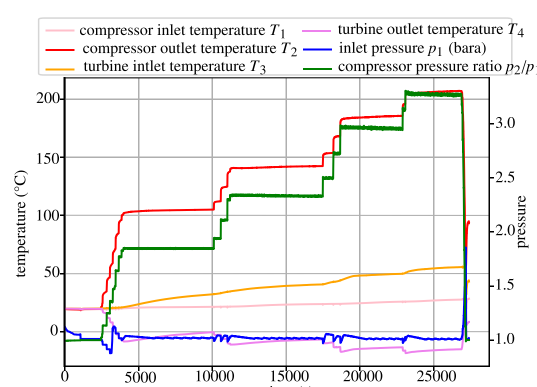

Fig. 16. Closed-loop operation of the CoBra. Pressure and temperature of turbo-machine components over the entire operation duration.

the compressor speed increases over time, an increasing heat output can be observed. The design operating point of the system is at a compressor power of approximately 55 kW. The motor drive power is about 63 kW, and thus, more than 10% of the electric power are lost during conversion, which can be attributed to mechanical losses in the bearing, gearbox and belt system. In order to minimize these losses, the DLR is currently working on a new project which aims for a compression system with a direct-drive. At the operating point, the steady-state heat flow of the HTHX is around 43 kW and that of the LTHX is roughly 15 kW. The turbine recovers about 26 kW of the fluid energy with an isentropic efficiency of about $\eta_{\mathrm{T,is}} = 75\%$. Differences in the heat flows to the HTHX (red) and from HTHX to the heat sink (pink) are due to transient heating of the HTHX. The difference in the heat flows

$$\dot{Q}_{\mathrm{HTHX,in}} - \dot{Q}_{\mathrm{HTHX,out}} = \frac{d}{dt}\left(m \cdot c_p \cdot T\right)_{\mathrm{HTHX}} + \dot{Q}_{\mathrm{HTHX,loss}} \tag{1}$$

must be equal to the change in thermal energy of the HTHX in addition to the thermal losses. With both heat flow rates approaching the same value after approximately an hour of operation in a constant operating regime we can conclude that thermal losses in the insulated HTHX are negligible once steady-state conditions are reached and that the transient phase until reaching steady-state operation without measurable parameter changes takes more than one hour.

The COP depicted here refers to the heat uptake in the sink $\dot{Q}_{\mathrm{HTHX,out}}$ in relation to the difference in fluid work of both, compressor power P_{C} and turbine power P_{T} which are calculated from the fluid enthalpy change assuming constant c_P, according to:

$$P_{\mathrm{C}} = \dot{m} \cdot c_{\mathrm{P}} \cdot \Delta T_{\mathrm{C}}; \Delta T_{\mathrm{C}} = T_2 - T_1, \tag{2}$$

$$P_{\mathrm{T}} = \dot{m} \cdot c_{\mathrm{P}} \cdot \Delta T_{\mathrm{T}}; \Delta T_{\mathrm{T}} = T_3 - T_4. \tag{3}$$

The power consumed by the auxiliary systems, the mechanic losses as well as conversion losses are not considered. Hence, the COP reaches a steady-state value of about COP= 1.35. Fig. 16 shows the inlet and outlet temperatures of the compressor and turbine as well as the compressor inlet pressure and the pressure ratio across both compressor stages. The compressors achieve a maximum temperature lift of ≈190 °C with a total pressure ratio of 3.2. The maximum temperature at compressor outlet of T_2 = 205 °C can provide heat sink outlet temperatures of ≈185 °C. Temperatures of ≈-10 °C are reached at the turbine outlet. For future tests with use of the recuperator the temperature lift or alternatively the COP are expected to improve significantly.

5. Conclusion and outlook

In this work the design and commissioning of the Brayton HTHP CoBra have been presented. First, the design choices were described for each component such as turbo machines, heat exchanger, auxiliary systems as well as control system and data acquisition. The initial design of the CoBra has been carried out with a different compression system with a higher drive power. Within the scope of this work the CoBra was operated using a compression system achieving a lower drive power, which was sufficient for the initial commissioning of the system. A detailed description of the step-by-step commissioning is provided. After completing the commissioning the CoBra was operated in a closed-loop for the first time. It was shown that a turbo-machine-driven Brayton heat pump can reach temperatures up to 205 °C at the compressor outlet and −10 °C at the turbine outlet in a closed-loop operation. At the time of writing, the system has already reached 260 °C and −30 °C, respectively. The experiments covering this pat will be presented in a dedicated publication in the near future.

As a next step, the current setup will be used to experimentally validate different control approaches such as fluid inventory control and reinforcement learning to enable a fast and transient load flexibility. Therefore, the CoBra will be equipped with two valves allowing for reducing and increasing the fluid inventory in the primary cycle.

Furthermore, a new compression system will be integrated into the CoBra to operate the test rig at full capacity. Therefore, an upcoming project utilizes a compressor from a turbocharger coupled with a direct-drive system which enable a compression power up to 300 kW.

CRediT authorship contribution statement

Fatma Cansu Yücel: Writing – original draft, Project administration, Methodology, Investigation, Formal analysis. **Johannes Oehler:** Writing – review & editing, Validation, Project administration, Methodology, Formal analysis, Data curation. **Maximilian Kriese:** Project administration. **Enrico Jende:** Project administration. **Nico Setzepfand:** Formal analysis. **Panagiotis Stathopoulos:** Writing – review & editing, Supervision, Project administration, Funding acquisition.

Declaration of competing interest

The authors declare that they have no known competing financial interests or personal relationships that could have appeared to influence the work reported in this paper.

Acknowledgments

The authors wish to thank the team CoBra Jonas Naumann, Justus Herbrich, Mario Tannert and Simone Hoffmann for their technical and administrative support. Furthermore, the authors wish to thank Eberhard Nicke and Leander Schleußfor their great contribution in the project. The is funded by an institutional funding of the German Aerospace Center.

Appendix. Example appendix section

Appendix text.

Data availability

Data will be made available on request.

References

[1] IEA, Renewables 2023, 2024, https://www.iea.org/energy-system/renewables. (Accessed 05 September 2024).
[2] IEA, Heating, 2024, https://www.iea.org/energy-system/buildings/heating. (Accessed 05 September 2024).
[3] H. Ritchie, Sector by sector: where do global greenhouse gas emissions come from? Our World Data (2020) https://ourworldindata.org/ghg-emissions-by-sector.
[4] B. Zühlsdorf, F. Bühler, M. Bantle, B. Elmegaard, Analysis of technologies and potentials for heat pump-based process heat supply above 150 C, Energy Convers. Manag.: X 2 (2019) 100011.
[5] J. Oehler, J.O. Gollasch, A.P. Tran, E. Nicke, Part load capability of a high temperature heat pump with reversed brayton cycle, in: 13th IEA Heat Pump Conference 2021 (HPC2020) Conference Proceedings, 2021.
[6] M. Götz, J. Lefebvre, F. Mörs, A.M. Koch, F. Graf, S. Bajohr, R. Reimert, T. Kolb, Renewable power-to-gas: A technological and economic review, Renew. Energy 85 (2016) 1371–1390.
[7] C. Arpagaus, F. Bless, M. Uhlmann, J. Schiffmann, S.S. Bertsch, High temperature heat pumps: Market overview, state of the art, research status, refrigerants, and application potentials, Energy 152 (2018) 985–1010.
[8] C. Bataille, M. Åhman, K. Neuhoff, L.J. Nilsson, M. Fischedick, S. Lechtenböhmer, B. Solano-Rodriquez, A. Denis-Ryan, S. Stiebert, H. Waisman, et al., A review of technology and policy deep decarbonization pathway options for making energy-intensive industry production consistent with the Paris agreement, J. Clean. Prod. 187 (2018) 960–973.
[9] P. Agreement, Paris agreement, in: Report of the Conference of the Parties to the United Nations Framework Convention on Climate Change (21st Session, 2015: Paris). Retrived December, vol. 4, no. 2017, HeinOnline, 2015, p. 2.
[10] G. Kosmadakis, Estimating the potential of industrial (high-temperature) heat pumps for exploiting waste heat in EU industries, Appl. Therm. Eng. 156 (2019) 287–298.
[11] A. Høeg, K. Løver, G. Vartdal, Performance of a high-temperature industrial heat pump, using helium as refrigerant, in: High-Temperature Heat Pump Symposium, Copenhagen, 2024.
[12] A. Längauera, B.A. Christian Rakuscha, Test results of a rotation heat pump and further developments, in: 13th IEA Heat Pump Conference, Jeju, 2021.

[13] T.-M. Tveit, U. Khan, R. Zevenhoven, Environmental impact of high temperature industrial heat pumps from a global warming potential (GWP) perspective, Ind. Effic. (2020) 14–16.
[14] AHEAD project, 2025, https://www.ait.ac.at/themen/efficiency-in-industrial-processes-systems/projekte/ahead-industriewaermepumpe-zur-dampferzeugung. (Accessed 15 April 2025).
[15] Push2Heat project, 2025, https://push2heat.eu/. (Accessed 15 April 2025).
[16] Spirit EU project, 2025, https://spirit-heat.eu/. (Accessed 13 March 2025).
[17] Solindarity EU project, 2025, https://solindarity.eu/. (Accessed 13 March 2025).
[18] Eeethos EU project, 2025, https://greenovate-europe.eu/eeethos-project-kicks-off-to-decarbonise-industrial-process-heating-with-innovative-technologies/. (Accessed 13 March 2025).
[19] G. Kröger, U. Siller, T. Moser, S. Hediger, Towards a highly efficient small scale turboshaft engine: Part I—Engine concept and compressor design, in: Turbo Expo: Power for Land, Sea, and Air, vol. 45615, American Society of Mechanical Engineers, 2014, V02BT45A015.
[20] A.S.A. Kompressor GmbH, Kompressor T1-520, 2024, https://asa-kompressor.com/produkte/asa-kompressor/kompressor-t1-520/. (Accessed 18 September 2024).
[21] A.S.A. Kompressor GmbH, Kompressor T1-316(HD), 2024, https://asa-kompressor.com/produkte/asa-kompressor/kompressor-t1-316/. (Accessed 18 September 2024).
[22] S. Senkova, O. Senkov, D. Miracle, Cryogenic and elevated temperature strengths of an Al- Zn- Mg- Cu alloy modified with Sc and Zr, Met. Mater. Trans. A 37 (2006) 3569–3575.
[23] A.P. Tran, P. Stathopoulos, Dynamic simulation and experimental validation of a high-temperature Brayton heat pump, Appl. Therm. Eng. 274 (2025) 126536.
[24] J. Oehler, A.P. Tran, P. Stathopoulos, Simulation of a safe start-up maneuver for a brayton heat pump, in: Turbo Expo: Power for Land, Sea, and Air, vol. 86014, American Society of Mechanical Engineers, 2022, V004T06A003.